

# Intrinsic Insulating Ground State in Transition Metal Dichalcogenide TiSe<sub>2</sub>

Daniel J. Campbell<sup>1</sup>, Chris Eckberg<sup>1</sup>, Peter Y. Zavalij<sup>2</sup>, and Johnpierre Paglione<sup>1,3</sup>

<sup>1</sup>*Center for Nanophysics and Advanced Materials,  
Department of Physics, University of Maryland,  
College Park, Maryland 20742, USA*

<sup>2</sup>*Department of Chemistry, University of Maryland,  
College Park, Maryland 20742, USA*

<sup>3</sup>*Canadian Institute for Advanced Research,  
Toronto, Ontario M5G 1Z8, Canada*

(Dated: May 25, 2022)

The transition metal dichalcogenide TiSe<sub>2</sub> has received significant research attention over the past four decades, in large part due to the uniqueness of its charge-ordered state. Different work has presented ways to suppress the charge density wave transition, vary low temperature resistivity by orders of magnitude, and stabilize magnetic or superconducting states. Here we give the results of a new synthesis technique whereby samples were grown in an argon gas environment at pressures as high as 180 bar. Above 100 K, the properties of these samples are unchanged from previous reports, but a hysteretic resistance region that begins around 80 K accompanied by insulating low temperature behavior are distinct from anything previously observed. This new feature is linked to a decrease in carrier concentration and may allow access to a nonmetallic ground state in a material long speculated to be an excitonic insulator.

## I. INTRODUCTION

TiSe<sub>2</sub> has received perhaps the most extensive investigation of any member of the transition metal dichalcogenide (TMD) family. As with other TMDs, weak van der Waals bonding along the *c*-axis means that relatively minor tweaks to unit cell size or interlayer dynamics can have dramatic effects on physical properties. In TiSe<sub>2</sub>, these changes are most evident in study of the charge density wave (CDW) that, under normal conditions, emerges at 200 K<sup>1</sup>. The TiSe<sub>2</sub> Fermi surface is not susceptible to nesting, a typical cause of charge ordering in TMDs<sup>2</sup>, so other explanations have been proposed: several variations of the Jahn-Teller effect<sup>3-5</sup> or an excitonic insulator state resulting from a small indirect band gap or overlap<sup>6</sup>. Recent experiment has given support to the latter scenario<sup>7,8</sup>. Despite this, TiSe<sub>2</sub> shows metallic low temperature behavior, with resistivities often much lower than the 300 K value.

Both the application of high pressure and the intercalation or substitution of new atoms to TiSe<sub>2</sub> can change the character of the CDW, typically suppressing it and in some cases leading to superconductivity or magnetic ordering<sup>9-16</sup>. In this paper, we present a way of bringing about new properties in TiSe<sub>2</sub> without the introduction of extrinsic atoms or a change in measurement conditions. By applying up to 180 bar of pressure with argon gas during the growth process, we have synthesized both single and polycrystals that exhibit a first-order transition below 100 K, together with a large increase in the magnitude of the Hall coefficient and low temperature resistance. This differs from the insulating behavior seen in substitution studies in that pressure-grown samples show the same transport, magnetic, and structural properties as typical TiSe<sub>2</sub> at higher temperatures. The fact that

pressure growth affects only low temperature behavior suggests that it may counteract a parasitic metallic component to the resistance, allowing for observation of an insulating, charge-ordered ground state.

## II. EXPERIMENTAL METHODS

TiSe<sub>2</sub> crystals are typically grown by chemical vapor transport (CVT) with excess Se or, preferably, I<sub>2</sub> as the transport agent<sup>1,12,17-19</sup>. For this study samples were grown at elevated pressure in a Morris HPS-3210 furnace [Fig. 1(a)], as has been done previously with the topological insulator Bi<sub>2</sub>Se<sub>3</sub><sup>20</sup>. This furnace can reach pressures up to 200 bar at 1000 °C by introducing Ar into a stainless steel growth chamber. The pressure in the chamber, as displayed on the furnace controller during the sequence, varies with temperature; the values reported here correspond to the maximum observed pressure for each growth, which (depending on maximum temperature) was about 60-70% larger than at room temperature.

It is not possible to do a traditional CVT growth in the pressure furnace, both because of the large amount of Ar gas present and the fact that iodine vapor would damage the chamber. So the actual process was closer to a “Se flux” method. Se shot (99.999+%, Alfa Aesar) and crushed Ti slugs (99.98%, Alfa Aesar) were mixed together at the bottom of a quartz ampule with a 40 cm length and 0.75 cm inner diameter. Growths were attempted with Ti-Se ratios ranging from 1:2 to 1:9, and several different temperature profiles. A typical sequence was to heat the furnace at 48 °C/hour to 600-700 °C and stay at the maximum temperature for 24-48 hours. The sample space was then slowly cooled at 4.8 °C/hour to

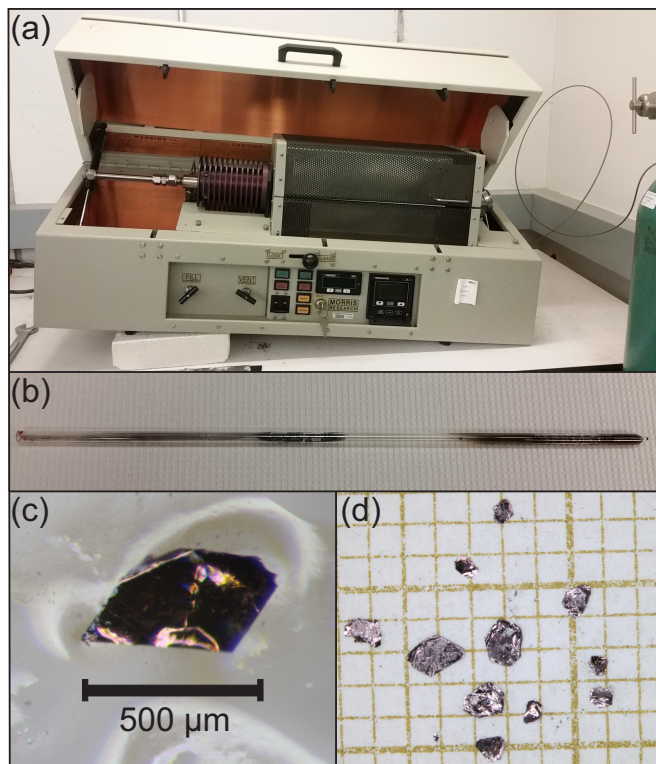


FIG. 1. (a) The Morris HPS-3210 furnace used for growth. A quartz ampule, open at one end, was inserted with its closed end on the right hand side near the heating element. The entire chamber was then sealed and the furnace lid closed. Tilting the furnace is suspected to help nucleate crystals. (b) A typical ampule after growth. The dark area on the closed right end is polycrystalline  $\text{TiSe}_2$ , while the region in the middle is elemental Se. (c) A small, fragile, pressure-grown  $\text{TiSe}_2$  crystal. (d) Larger pressure-grown  $\text{TiSe}_2$  single crystals (on  $1 \times 1 \text{ mm}^2$  scale paper), which had a different appearance and were less common.

400 °C, at which point the furnace was turned off and passively cooled to room temperature; only then was the chamber returned to ambient pressure. For comparison, we also growth single crystals via CVT with  $\text{I}_2$ , and a flux technique<sup>21</sup> using excess Se (at a 1:9 ratio with Ti) in alumina crucibles in about 1/3 atm of Ar gas inside a sealed quartz tube.

All pressure furnace growths produced a large number of polycrystalline chunks, but only about half also resulted in single crystals large enough for transport measurements. Other growths produced some single crystals less than 200  $\mu\text{m}$  across. There was no identifiable correspondence between growth pressure, temperature profile, or Ti-Se ratio and the successful production of large crystals. Empirically, it seemed that propping up the cooler end of the furnace at an angle helped to form crystals, as was also noticed in the case of  $\text{Bi}_2\text{Se}_3$ <sup>20</sup>. This may have been because it concentrated Se at the end of the ampule where the Ti slugs were located, since the excess Se would often condense further up the length of the tube

upon opening the growth [Fig. 1(b)]. It could also have helped to amplify any temperature gradient in the furnace and approximate the conditions for vapor transport.

Resultant single crystals also varied in appearance between growths, as seen in Figs. 1(c) and 1(d). Some were small, wispy, and flexible, less than half a millimeter in length and 15-60  $\mu\text{m}$  in thickness. Others were larger and sturdy, over 1 mm wide and 200  $\mu\text{m}$  thick. In either case, single crystal x-ray diffraction (XRD) confirmed that the platelike crystals always grew with the  $c$ -axis out of plane, as would be expected for hexagonal, layered  $\text{TiSe}_2$ .

Synchrotron powder x-ray diffraction (XRD) patterns of ground polycrystals were obtained through the beamline 11-BM mail-in program at the Advanced Photon Source at Argonne National Laboratory, and refinements were made with the GSAS-II software package<sup>22</sup>. High quality single crystal measurements were also made at 150 K on a Bruker APEX2 Diffractometer with  $\text{Mo K}\alpha$  radiation. The integral intensities were corrected for absorption using the SADABS software<sup>23</sup> using the integration method. The structure was solved with the ShelXS-2015 program and refined with the ShelXL-2015 program and least-square minimization using the ShelX software package<sup>24</sup>. Electrical transport measurements were carried out in 9 T and 14 T Quantum Design Physical Properties Measurement Systems, and 14 T Quantum Design DynaCool. The 14 T PPMS and DynaCool systems were used for heat capacity measurements. Magnetization was measured using the DynaCool vibrating sample magnetometer as well as two versions of the 7 T Quantum Design Magnetic Properties Measurement System, the MPMS XL and MPMS3.

### III. PHYSICAL PROPERTIES

#### A. Structural Characterization

Room temperature synchrotron diffraction patterns were taken of ground polycrystals from seven growths: CVT (0 bar), Se flux (1 bar), and five pressure growths in the range 56-160 bar. A refined pattern for a 130 bar growth is shown in Fig. 2(a), with the volumes and lattice parameters of all refinements presented in Figs. 2(b) and 2(c). Lattice parameters were in the range  $3.5387 < a < 3.5400 \text{ \AA}$  and  $6.0065 < c < 6.0099 \text{ \AA}$ . These numbers are very close to reference values<sup>11,19</sup>, and comparable to reports for crystals with < 5% of various intercalants or dopants<sup>10,11,14,16</sup>. Overall, samples grown at pressure show minimal lattice change at room temperature. Elemental Se was also found at low levels in some powder diffraction patterns, presumably a result of the excess material used in the growth.

Five single crystal samples grown in the range 101-140 bar were also selected for XRD at 150 K [Table I]. However, these data are not directly comparable to room temperature values as they are determined by a combination of thermal contraction and CDW-related lattice dis-

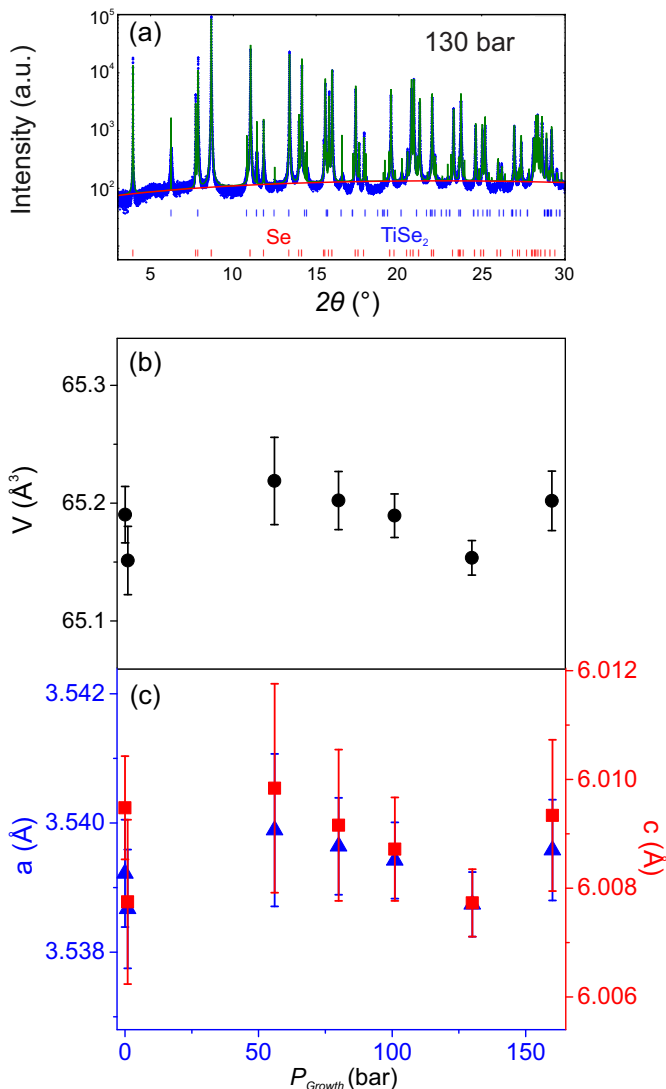


FIG. 2. (a) Experimental (blue) and simulated (green) patterns for a 130 bar growth obtained from synchrotron powder diffraction, with a logarithmic y-axis. The red line is the subtracted background, and hashes underneath indicate the location of elemental Se (red) and  $\text{TiSe}_2$  (blue) peaks. We also present the volumes (b) and lattice parameters (c) vs. growth pressure (with error bars) from refinement of all synchrotron data. CVT and Se flux growths are referred to as 0 and 1 bar, respectively.

tortion. What they demonstrate, however, is that  $T_{\text{CDW}}$  is above 150 K for these samples. This is in spite of different growth conditions and varied low temperature resistivities, which were 2-5 times higher than the 300 K value. Using the reported  $\text{TiSe}_2$  lattice parameters<sup>19</sup> and thermal expansion coefficients<sup>25</sup> we can estimate that at 150 K, before accounting for the effect of the CDW on the lattice,  $a = 3.530$  Å and  $c = 5.993$  Å for typical  $\text{TiSe}_2$ . Instead, we see 150 K lattice parameters that are, with the exception of the 140 bar sample, similar to or larger than room temperature values. The explana-

TABLE I. Parameters obtained from refinements of 150 K single crystal XRD measurements. Two crystals from the same 101 bar growth were selected.

$P_{\text{Growth}}$ (bar)	$a$ (Å)	$c$ (Å)	$wR_2$
101 #1	3.5415(11)	6.0198(19)	0.0494
101 #2	3.5355(9)	6.0112(16)	0.0556
114	3.5332(15)	6.007(3)	0.0553
138	3.5432(10)	6.0195(17)	0.0615
140	3.5275(11)	5.9969(19)	0.0509

tion for the lattice expansion is charge ordering, which at 150 K can cause a distortion of more than  $10^{-2}$  Å in typical  $\text{TiSe}_2$ <sup>1,26</sup>. Pressure growth does not have a substantial effect on charge ordering, since by 150 K samples that have clearly undergone a lattice expansion due to CDW formation.

Energy-dispersive x-ray spectroscopy (EDS) confirms a Se deficiency in the vast majority of samples, despite the use of excess material in the growth. Individual samplings have a relatively large uncertainty, but combining results for multiple growths we get an average Se:Ti ratio of  $1.82 \pm 0.05$ . This is a larger deficiency than would be expected based on growth temperature<sup>1,27</sup>. However, similar levels of Se deficiency were found samples grown with the standard  $\text{I}_2$  CVT method, meaning that any novel behavior accompanying pressure growth is not simply a result of nonstoichiometry.

## B. Electrical Transport

The temperature-dependent resistance of a number of single crystals grown at various pressures are shown in Fig. 3, with resistances scaled to 300 K values. Above 100 K, the behavior does not differ from previous reports on  $\text{TiSe}_2$ . In line with previous convention we used the kink in the derivative (a peak in the second derivative) as indicating the onset of charge ordering<sup>1</sup>. The values we see for all samples are just above 200 K, the same as standard  $\text{TiSe}_2$ . All samples have a rise upon cooling at 200 K regardless of behavior at lower temperatures. On the other hand, the peak in resistance, normally centered around 165 K, is lower in most of our samples. A similar effect has been reported in samples grown without  $\text{I}_2$ <sup>28</sup>, or by varying growth temperature<sup>1,27</sup>, and is thought to be linked to nonstoichiometry. The ratio  $R_{\text{peak}}/R(300 \text{ K})$  for our samples can be as high as seven, much larger than has been achieved with CVT crystal growth<sup>27,28</sup>. An increased relative peak height has previously been thought to correspond to fewer Se vacancies and correspondingly higher crystal quality<sup>1,17,29</sup>. However, this was only an assumption in those papers, and in fact a more recent paper has even argued that Se deficiency is actually beneficial to charge ordering<sup>27</sup>. Our crystals show a taller peak at a lower temperature with an appreciable Se deficiency. We therefore discard any notion of correspon-

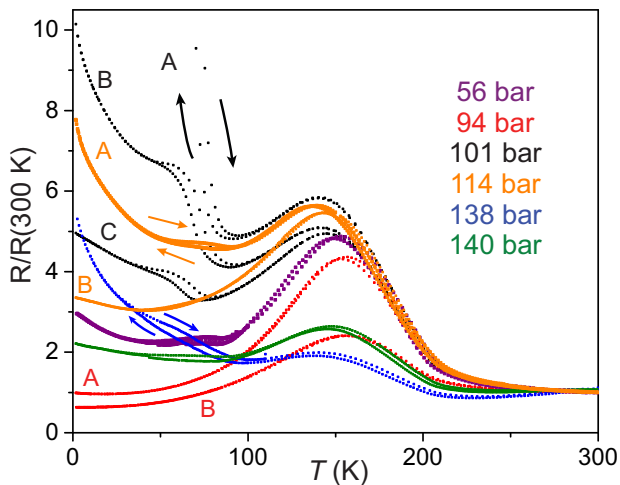


FIG. 3. Resistance (scaled to 300 K value) as a function of temperature for  $\text{TiSe}_2$  single crystals, with maximum growth pressures noted. Samples from the same growth are distinguished by lettering. Arrows indicate the direction of temperature sweeps, showing hysteresis that is also noticeable in data without arrows.

dence between the peak's height, its temperature, and crystal quality.

At lower temperatures many pressure-grown samples show a large increase in resistivity with decreasing temperature, a significant departure from expected behavior. Additionally, temperature hysteresis often opens around 80 K in a similar range to where insulating character emerges. This is emphasized in Fig. 4, which shows  $\Delta R$ , defined as the difference in resistance value between warming and cooling, scaled to its room temperature value, for five samples from a single 101 bar growth. In most cases the greatest hysteresis occurs between 50-100 K, with some samples also showing large values near the higher temperature local maximum where resistance changes most quickly. This effect is present both when temperature is swept slowly and continuously or stabilized at each data point. Application of fields up to 140 kOe did not change overall behavior, and even for measurements of longitudinal resistance the Hall component was often dominant enough to obscure any small magnetoresistive signal. Similar results were seen for both single crystal and polycrystalline samples, but we present only single crystal resistance data in order to demonstrate that the effect is inherent to pressure-grown  $\text{TiSe}_2$  and not a result of insulating impurities, grain boundaries, or other effects that make polycrystalline transport measurements less reliable.

While polycrystals were universally insulating at low temperatures, not all single crystals showed the 80 K transition; some behaved like typical, CVT-grown  $\text{TiSe}_2$ , and behavior below 100 K varied even for samples from the same growth with similar room temperature resistivities [Fig. 4, inset]. The height of the CDW peak was also inconsistent and  $T_{\text{peak}}$  could vary by 10 K. The

lowest growth pressure to produce single crystals was 56 bar, and the highest was 140 bar, but polycrystals grown at maximum pressures of 10-180 bar behaved similarly. While pressure synthesis conditions are necessary to stimulate this behavior, there does not seem to be a clear relationship between the exact growth pressure and the specifics of low temperature behavior. In general there was no identifiable link between any physical properties and particular growth pressure. The location of material within the ampule and the obscurities of crystal nucleation in a high gas pressure environment, which are much harder to track, are likely more relevant.

A comparison of  $\rho(T)$  for crystals grown by  $\text{I}_2$  CVT, Se flux, and Ar pressure [Fig. 5(a)] makes clearer the differences between the techniques. Resistivity values are initially similar, and all show the CDW-associated rise in  $\rho$  at a similar temperature. The CVT crystal has a peak at 165 K and  $\rho(1.8 \text{ K}) < \rho(300 \text{ K})$ . The Se flux sample has a suppressed  $T_{\text{peak}}$  of 150 K and slightly higher resistivity at 1.8 K than room temperature. A pressure-grown crystal has a local maximum at even lower temperature (140 K) and a hysteretic, insulating transition.  $T_{\text{CDW}}$  has typically been identified as the beginning of the flat minimum region in the first derivative<sup>1</sup>. However, as can be seen in Fig. 5(a) the minima for Se flux and pressure-grown samples are influenced by the suppression of  $T_{\text{peak}}$ . We therefore used the peak in the second derivative, equivalent to the kink in the first derivative, to define  $T_{\text{CDW}}$ . The inset to Fig. 5(b) clearly demonstrates that this occurs at the same temperature for all three samples. While both Se flux and pressure-grown crystals have an elevated low temperature resistance compared to CVT samples, the insulating behavior is much larger in those grown under pressure and also features hysteresis.

As with longitudinal resistivity, the Hall resistance [Fig. 6(a)] in pressure-grown crystals above 200 K is generally similar to typical  $\text{TiSe}_2$ <sup>1</sup>. The Hall coefficient  $R_{\text{H}}$  is initially positive and crosses zero near 165 K. Similar to the peak in  $\rho(T)$ , this is at a slightly lower temperature than previous reports<sup>1,28</sup> and varies between samples, but not as substantial a drop as seen upon elemental substitution<sup>30,31</sup>. At low temperatures  $R_{\text{H}}$  can reach large negative values up to two orders of magnitude larger than those of typical  $\text{TiSe}_2$ <sup>1</sup> and an order of magnitude above those measured even for insulating  $\text{Ti}_{1-x}\text{M}_x\text{Se}_2$  ( $\text{M} = \text{As}, \text{Sc}, \text{Nb}, \text{Ni}, \text{Re}, \text{or Y}$ )<sup>31</sup>. This indicates a different mechanism for insulating behavior in pressure-grown samples: a reduced carrier concentration rather than impurity scattering. The inset to Fig. 6(a) compares the scaled resistance and  $-R_{\text{H}}$  at low temperatures. Generally, samples with more insulating low temperature behavior had a reduced carrier concentration.

### C. Heat Capacity

Heat capacity measurements were taken from 300 K to 2 K on a polycrystalline chunk of  $\text{TiSe}_2$  grown at

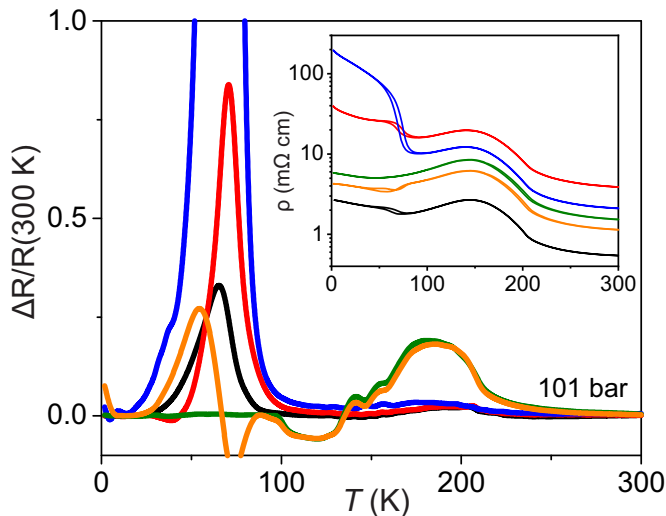


FIG. 4.  $\Delta R \equiv R_{\text{warming}} - R_{\text{cooling}}$ , scaled to room temperature resistance, as a function of temperature for five crystals from a single 101 bar growth. Hysteresis is most evident around 80 K but also manifests at the higher temperature CDW resistance peak.  $\Delta R/R$  reaches a maximum of 7 for the blue curve, and a minimum of -0.15 for the orange curve. Inset:  $\rho(T)$  of each sample, with matching colors.

160 bar [Fig. 6(b)], which had shown an insulating transition in transport measurements. However, there are no features in the corresponding temperature range, and the shape and values of the data are very similar to what has been measured before for CVT-grown  $\text{TiSe}_2$ <sup>29</sup>. The lack of a feature in the hysteretic region is not wholly surprising, as even the higher temperature CDW has only a very subtle effect. Low temperature measurements on the same polycrystal and two others grown at different pressures are shown in the inset to Fig. 6(b). All data fit well to the standard specific heat equation  $C/T = \gamma + \beta T^2$ . In this equation,  $\gamma$  is the Sommerfeld coefficient and  $\beta$  can be used to calculate the Debye temperature  $\theta_D = (\frac{12\pi^4 N_A k_B n}{5\beta})^{\frac{1}{3}}$ , where  $N_A$  is the Avogadro number,  $k_B$  Boltzmann's constant, and  $n = 3$  the number of atoms per formula unit. Results were similar for all three samples. The computed  $\gamma$  values are small: 0.14, 0.16, and 0.19  $\frac{\text{mJ}}{\text{mol K}^2}$  respectively for the 98, 130, and 160 bar samples, reflecting the the small low temperature density of states at the Fermi energy.  $\theta_D$  is 220, 244, and 209 K for the same data. The values for  $\text{TiSe}_2$  powder<sup>29</sup> are  $\gamma = 0.19 \frac{\text{mJ}}{\text{mol K}^2}$  and  $\theta_D = 251$  K. The lower  $\theta_D$  in pressure-grown samples may indicate phonon softening related to an enhancement of charge ordering.

#### D. Magnetic Susceptibility

Like heat capacity, magnetization measurements [Fig. 6(c)] differed little from vapor transport-grown  $\text{TiSe}_2$ . Pressure-grown polycrystals show both positive and negative  $\chi$  values which are small in either case,

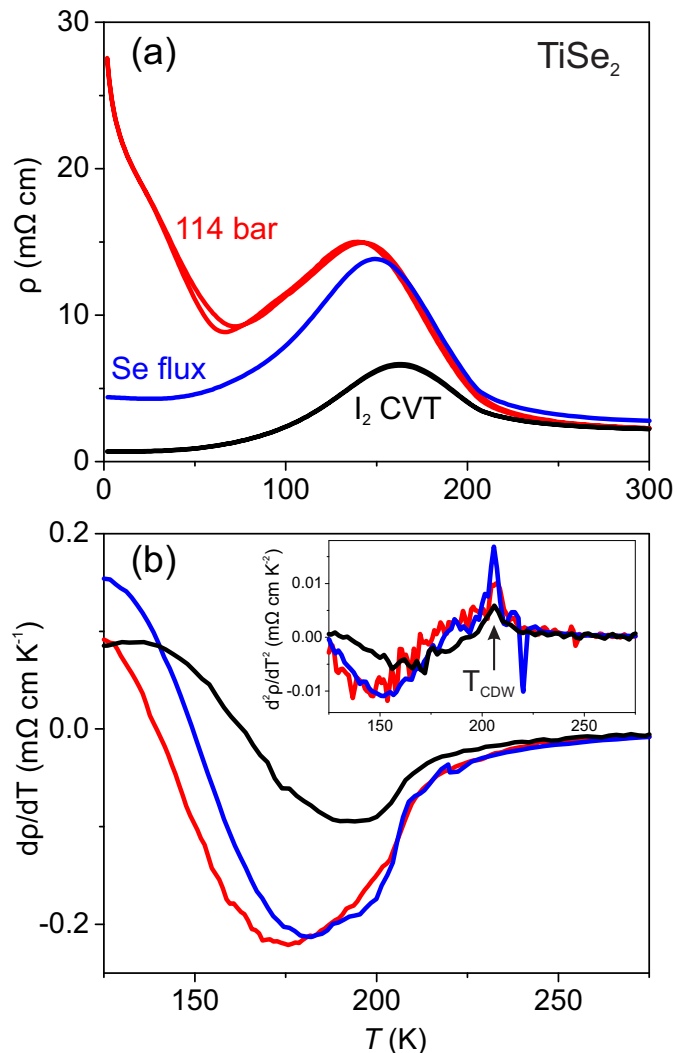


FIG. 5. (a) Temperature-dependent resistivity for  $\text{TiSe}_2$  single crystals grown by  $\text{I}_2$  chemical vapor transport, excess Se flux, and 114 bar of pressure applied with Ar gas. At high temperatures the behavior of all three samples is similar, but differences emerge below 150 K. No hysteresis is observed in the CVT or flux crystals. (b) The derivative of the cooling data from (a) in a narrower temperature region. (inset) The second derivative of the same data. The peak is identified as the onset of the CDW.

roughly  $10^{-5} \frac{\text{emu}}{\text{mol Oe}}$ . The shape matches both powder data<sup>1</sup> and results from our own CVT-grown samples. A knee and drop in  $\chi(T)$ , with a similar shape to  $d\rho/dT$ , is linked to the CDW onset. A plateau is seen at lower temperatures, before paramagnetic impurities (subtracted from Ref. 1) cause a rise at lowest temperatures. Data were taken under large fields ( $\geq 50$  kOe) to enhance the weak signal, but curves had the same appearance over the range 0-140 kOe.

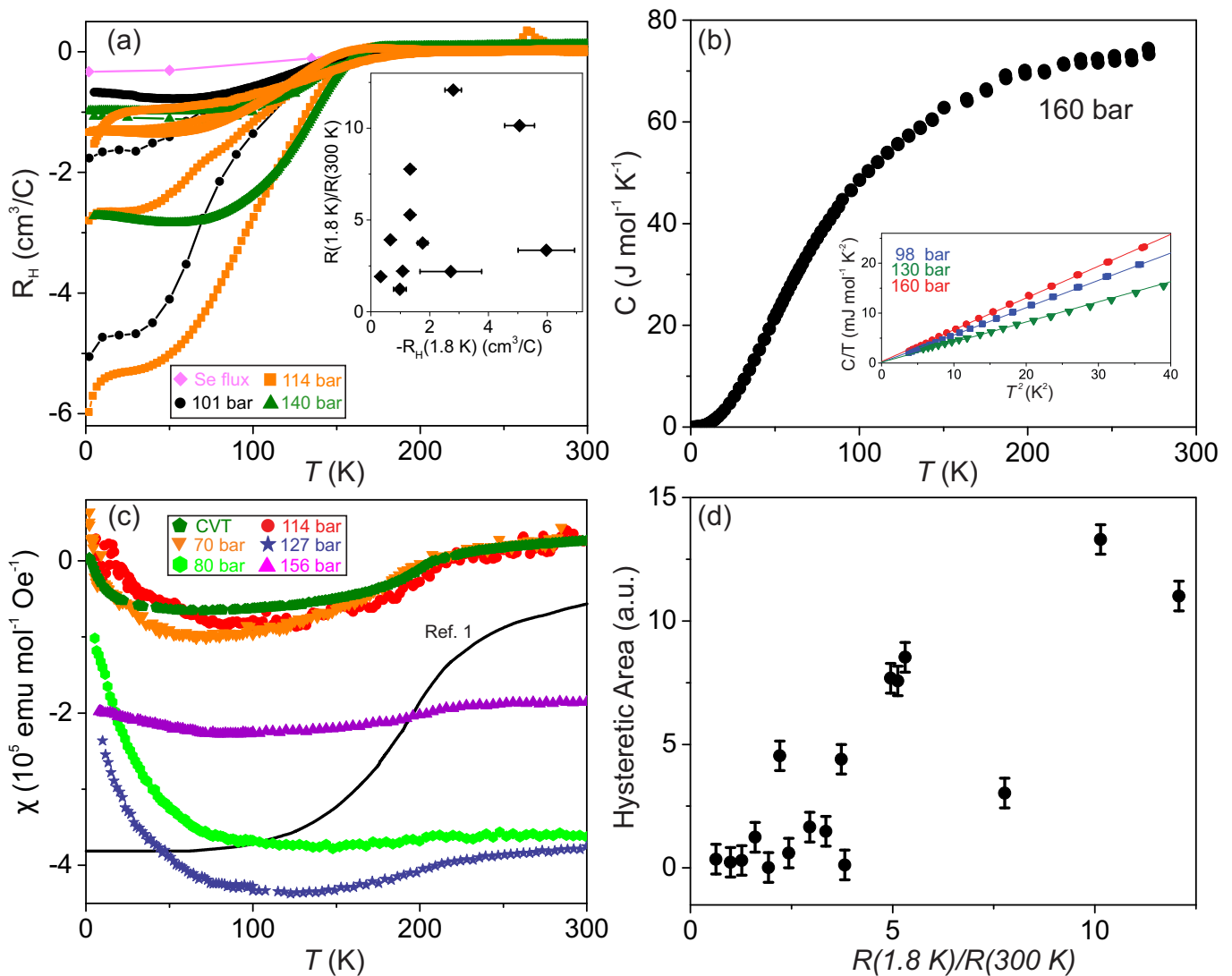


FIG. 6. (a) The temperature dependence of the Hall coefficient of TiSe<sub>2</sub> single crystals. Inset: the increase in resistance at base temperature scaled to 300 K value plotted against the negative Hall coefficient at base temperature. More insulating samples generally showed a larger  $|R_H|$ . Error bars come from uncertainty in the measurement of sample thickness. (b) Specific heat of a polycrystalline TiSe<sub>2</sub> sample with a maximum growth pressure of 160 bar as a function of temperature. Inset: Low temperature data for the same sample and two other polycrystals, with maximum growth pressures noted. Lines are fits to the Debye low temperature specific heat model. (c) Magnetic susceptibility for polycrystalline TiSe<sub>2</sub> chunks taken in constant applied fields of 50 or 70 kOe, compared to powder data from Di Salvo *et al.*<sup>1</sup> (d) The hysteretic area (see Discussion for details) versus resistance increase for pressure-grown single crystals. Error bars are based on the difference from zero for non-hysteretic samples.

#### IV. DISCUSSION

Above about 100 K, there is no difference in the behavior of TiSe<sub>2</sub> grown with iodine vapor or at high pressure. The sudden decrease in  $\chi(T)$  and the maximum in  $d^2\rho/dT^2$  (the  $d\rho/dT$  inflection point) have both been connected to the onset of charge ordering<sup>1,30</sup>. These occur at the same temperature, within 5 K, for pressure-grown TiSe<sub>2</sub> compared to CVT samples, despite dramatic differences in lower temperature resistivity in many single crystals, even those from the same growth. The

distinct aspect of pressure growth is the lower temperature transport behavior. While TiSe<sub>2</sub> becomes more insulating with V doping ( $\leq 5\%$ )<sup>9,30</sup> or the intercalation of Cr, Fe, Co, and (in small quantities, before leading to superconductivity) Pd<sup>10,14,15</sup>, the resistivity of those samples is not hysteretic. Furthermore, they show a more significant change in room temperature lattice parameters<sup>10,11,14,16</sup>, CDW suppression<sup>13</sup>, and antiferromagnetic or Curie-Weiss behavior<sup>10</sup>. On the other hand, Ti<sub>1-x</sub>Pt<sub>x</sub>Se<sub>2</sub> does have some similarities to our findings. Up to  $x = 0.13$ , it increases  $\rho$  by eight orders of

magnitude at low temperatures, while lattice constants at 300 K and  $T_{\text{CDW}}$  hardly change<sup>15</sup>. However, there is no hysteresis reported. Transport measurements and density functional theory calculations attribute this change to an increased energy gap. Pressure growth may similarly influence the band structure, as is thought to be the case for pressure-grown  $\text{Bi}_2\text{Se}_3$ <sup>20</sup>.

CVT-grown  $\text{TiSe}_2$  has shown both metallic<sup>1,27</sup> or semimetallic<sup>11,14,15</sup> resistive behavior, without explanation or even much recognition of this variation. Our own CVT or Se flux crystals can similarly differ in low temperature properties [Fig. 5(a)]. Whether  $\text{TiSe}_2$  has a semimetallic or semiconducting band structure is ambiguous<sup>32</sup>, but a CDW transition would typically be expected to lead to more insulating behavior<sup>2</sup>. Exciton condensation would also remove carriers from both electron and hole bands. Because we observe a decrease in carrier concentration that is more dramatic in more insulating samples [Fig. 6(a), inset], we conclude that pressure growth of  $\text{TiSe}_2$  makes it possible to observe a truly insulating charge ordered ground state, which carries with it a hysteretic transition. In Fig. 6(d) we plot the “hysteretic area” of single crystal samples against their scaled resistance increase,  $R(1.8\text{ K})/R(300\text{ K})$ . This quantity is defined as the area under the  $\Delta R/R(300\text{ K})$  vs.  $T$  curve between 30 and 80 K. The error bar comes from the largest area seen in non-hysteretic samples, which ideally would have vanishing hysteresis. There is a clear connection between more insulating low temperature behavior and more pronounced hysteresis, even after scaling to raw resistance values.

Other TMDs display multiple transitions of varying insulating character.  $\text{TaS}_2$  has three progressively more insulating CDW transitions, with the two at lower temperature being hysteretic<sup>33,34</sup>. They correspond to the onset of (with decreasing temperature) incommensurate, nearly commensurate, and fully commensurate CDWs. Thus it would not be unusual to see something similar in  $\text{TiSe}_2$ . Beyond emphasizing the conduction channel associated with the charge-ordered state, another possibility is that pressure growth introduces a slight incommensuration of the 200 K CDW. Recent reports on superconducting Cu-intercalated or pressurized samples observe incommensurate CDWs in certain regions of the phase diagram just above the superconducting transition, and attribute them to  $c$ -axis stacking faults<sup>35–37</sup>. Pressure applied during growth may affect the lattice during crystallization, and the lower temperature feature could be a “lock-in” to full commensuration, as occurs near 200 K in  $\text{TaS}_2$ <sup>34</sup> and 100 K in  $\text{TaSe}_2$ <sup>38</sup>. The ICDW-CCDW transitions in Cu-intercalated or pressurized samples occur in the 70-80 K range<sup>36,37</sup>, also where pressure-grown samples first show hysteresis. X-ray measurements indicate that this transition is first order in pressurized  $\text{TiSe}_2$  and should therefore be hysteretic. Still, both applied pressure and Cu intercalation lower  $T_{\text{CDW}}$  and induce metallicity, unlike pressure growth. For that reason

we believe that pressure growth might reveal an intrinsic phase previously unnoticed in  $\text{TiSe}_2$ , rather than a new phenomenon. Future work with x-ray scattering or scanning tunneling microscopy would be highly valuable in pinning down the source of this unprecedented low temperature transition.

## V. CONCLUSION

Our work is the first report of insulating behavior in  $\text{TiSe}_2$  without substitution or intercalation. Instead, samples grown under argon gas pressures of 10-180 bar frequently showed a much larger resistance and reduced carrier concentration at low temperatures. Prior examples in which the introduction of new atoms caused a low temperature resistance increase lack the hysteretic behavior that we have observed starting around 80 K. The cause of this newly observed transition is still unknown, but we suspect it is associated with an enhancement of charge ordering and suppression of a metallic component that dominates transport behavior in crystals grown by vapor transport. This first order transition may be a signature of the charge-ordered, excitonic insulator ground state of  $\text{TiSe}_2$ , or could also indicate a subtle change to the higher temperature commensurate CDW.

Due to their weak interlayer bonding, applied pressure or chemical substitution can significantly impact the behavior of transition metal dichalcogenides. We have presented another method, high pressure synthesis. Going forward, it will be important to identify the root of this novel low temperature behavior through further physical characterization, in the hopes of finding a new way to tune this well-studied system. The association between weakening of charge ordering in  $\text{TiSe}_2$  and superconductivity, demonstrated by the observation of CDW incommensuration near a quantum critical point in pressurized or Cu-intercalated samples, is another reason to further explore high pressure crystal growth. This same material growth technique could also lead to new discoveries in the wider family of TMDs or other materials with unstable lattice configurations.

## VI. ACKNOWLEDGMENTS

This work was supported by Air Force Office of Scientific Research award no. FA9550-14-1-0332, National Science Foundation Division of Materials Research award no. DMR-1610349, and the Gordon and Betty Moore Foundation’s EPiQS Initiative through grant no. GBMF4419. D.J.C. was funded in part by the U.S. Department of Energy, Office of Science, Office of Workforce Development for Teachers and Scientists, Office of Science Graduate Student Research program. The SCGSR program is administered by the Oak Ridge Institute for Science and Education for the DOE under contract no. DESC0014664. Use of the Advanced Photon

Source at Argonne National Laboratory was supported by the DOE, Office of Science, Office of Basic Energy

Sciences, under contract no. DE-AC02-06CH11357. We also acknowledge the support of the Maryland NanoCenter and its FabLab.

- 
- <sup>1</sup> F. J. Di Salvo, D. Moncton, and J. Waszczak, *Phys. Rev. B* **14**, 4321 (1976).
- <sup>2</sup> K. Rossnagel, *J. Phys.-Condens. Mat.* **23**, 213001 (2011).
- <sup>3</sup> H. Hughes, *J. Phys. C: Solid State* **10**, L319 (1977).
- <sup>4</sup> M. H. Whangbo and E. Canadell, *J. Am. Chem. Soc.* **114**, 9587 (1992).
- <sup>5</sup> J. van Wezel, P. Nahai-Williamson, and S. S. Saxena, *Phys. Rev. B* **81**, 165109 (2010).
- <sup>6</sup> D. Jérôme, T. M. Rice, and W. Kohn, *Phys. Rev.* **158**, 462 (1967).
- <sup>7</sup> H. Cercellier, C. Monney, F. Clerc, C. Battaglia, L. Despont, M. G. Garnier, H. Beck, P. Aebi, L. Patthey, H. Berger, and L. Forró, *Phys. Rev. Lett.* **99**, 146403 (2007).
- <sup>8</sup> A. Kogar, M. S. Rak, S. Vig, A. A. Husain, F. Flicker, Y. I. Joe, L. Venema, G. J. MacDougall, T. C. Chiang, E. Fradkin, J. van Wezel, and P. Abbamonte, *Science* **358**, 1314 (2017).
- <sup>9</sup> F. J. Di Salvo and J. V. Waszczak, *Phys. Rev. B* **17**, 3801 (1978).
- <sup>10</sup> A. Kuranov, V. Pleshchev, A. Titov, N. Baranov, and L. Krasavin, *Phys. Solid State+* **42**, 2089 (2000).
- <sup>11</sup> E. Morosan, H. Zandbergen, B. Dennis, J. Bos, Y. Onose, T. Klimczuk, A. Ramirez, N. Ong, and R. Cava, *Nat. Phys.* **2**, 544 (2006).
- <sup>12</sup> A. F. Kusmartseva, B. Sipos, H. Berger, L. Forro, and E. Tutiš, *Phys. Rev. Lett.* **103**, 236401 (2009).
- <sup>13</sup> M. Sasaki, A. Ohnishi, T. Kikuchi, M. Kitaura, K. Shimada, and H.-J. Kim, *J. Low Temp. Phys.* **161**, 375 (2010).
- <sup>14</sup> E. Morosan, K. E. Wagner, L. L. Zhao, Y. Hor, A. J. Williams, J. Tao, Y. Zhu, and R. J. Cava, *Phys. Rev. B* **81**, 094524 (2010).
- <sup>15</sup> J. S. Chen, J. K. Wang, S. V. Carr, S. C. Vogel, O. Gourdon, P. Dai, and E. Morosan, *Phys. Rev. B* **91**, 045125 (2015).
- <sup>16</sup> H. Luo, J. W. Krizan, E. M. Seibel, W. Xie, G. S. Saahasrabudhe, S. L. Bergman, B. F. Phelan, J. Tao, Z. Wang, J. Zhang, and R. J. Cava, *Chem. Mater.* **27**, 6810 (2015).
- <sup>17</sup> B. Hildebrand, C. Didiot, A. M. Novello, G. Monney, A. Scarfato, A. Ubal dini, H. Berger, D. R. Bowler, C. Renner, and P. Aebi, *Phys. Rev. Lett.* **112**, 197001 (2014).
- <sup>18</sup> D. B. Lioi, D. J. Gosztola, G. P. Wiederrecht, and G. Karapetrov, *Appl. Phys. Lett.* **110**, 081901 (2017).
- <sup>19</sup> C. Riekkel, *J. Solid State Chem.* **17**, 389 (1976).
- <sup>20</sup> P. Syers and J. Paglione, *Phys. Rev. B* **95**, 045123 (2017).
- <sup>21</sup> P. C. Canfield and Z. Fisk, *Philos. Mag. B* **65**, 1117 (1992).
- <sup>22</sup> B. H. Toby and R. B. Von Dreele, *J. Appl. Crystallogr.* **46**, 544 (2013).
- <sup>23</sup> L. Krause, R. Herbst-Irmer, G. M. Sheldrick, and D. Stalke, *J. Appl. Crystallogr.* **48**, 3 (2015).
- <sup>24</sup> G. M. Sheldrick, *Acta Crystallogr. C* **71**, 3 (2015).
- <sup>25</sup> G. Wiegers, *Physica B + C* **99**, 151 (1980).
- <sup>26</sup> C. Monney, C. Battaglia, H. Cercellier, P. Aebi, and H. Beck, *Phys. Rev. Lett.* **106**, 106404 (2011).
- <sup>27</sup> S. Huang, G. Shu, W. W. Pai, H. Liu, and F. Chou, *Phys. Rev. B* **95**, 045310 (2017).
- <sup>28</sup> I. Taguchi, M. Asai, Y. Watanabe, and M. Oka, *Physica B + C* **105**, 146 (1981).
- <sup>29</sup> R. Craven, F. Di Salvo, and F. Hsu, *Solid State Commun.* **25**, 39 (1978).
- <sup>30</sup> F. Levy, *J. Phys. C: Solid State* **12**, 3725 (1979).
- <sup>31</sup> F. Levy, *J. Phys. C Solid State* **13**, 2901 (1980).
- <sup>32</sup> J. C. E. Rasch, T. Stemmler, B. Müller, L. Dudy, and R. Manzke, *Phys. Rev. Lett.* **101**, 237602 (2008).
- <sup>33</sup> A. Thompson, R. Gamble, and J. Revelli, *Solid State Commun.* **9**, 981 (1971).
- <sup>34</sup> B. Sipos, A. F. Kusmartseva, A. Akrap, H. Berger, L. Forró, and E. Tutiš, *Nat. Mater.* **7**, 960 (2008).
- <sup>35</sup> S. Yan, D. Iai, E. Morosan, E. Fradkin, P. Abbamonte, and V. Madhavan, *Phys. Rev. Lett.* **118**, 106405 (2017).
- <sup>36</sup> A. Kogar, G. A. de la Pena, S. Lee, Y. Fang, S.-L. Sun, D. B. Lioi, G. Karapetrov, K. D. Finkelstein, J. P. Ruff, P. Abbamonte, and S. Rosenkranz, *Phys. Rev. Lett.* **118**, 027002 (2017).
- <sup>37</sup> Y. I. Joe, X. Chen, P. Ghaemi, K. Finkelstein, G. de La Peña, Y. Gan, J. Lee, S. Yuan, J. Geck, G. MacDougall, T. Chiang, S. Cooper, E. Fradkin, and P. Abbamonte, *Nat. Phys.* **10**, 421 (2014).
- <sup>38</sup> R. M. Fleming, D. E. Moncton, D. B. McWhan, and F. J. Di Salvo, *Phys. Rev. Lett.* **45**, 576 (1980).